Active Control of Combustion Instabilities in Lean Premixed Combustors

Kwanwoo Kim, Christopher M. Jones, Jong G. Lee and Domenic A. Santavicca

The Pennsylvania State University

Abstract

Results are presented from two experimental studies of active control of combustion instabilities in lean-premixed laboratory-scale combustors using closed-loop secondary fuel modulation. In the first study, the use of subharmonic secondary fuel injection is investigated where it was demonstrated that effective control can be achieved at certain operating conditions with noise level reductions of up to 22 dB. In the second study, the effect of the spatial and temporal distribution of modulated secondary fuel on suppressing unstable combustion is evaluated for two different instabilities. Two-dimensional chemiluminescence measurements are made to characterize the evolution of the heat release during unstable combustion, while laser induced fluorescence is used to determine the spatial and temporal distribution of the injected secondary fuel. These measurements are used to calculate the Rayleigh Index Distribution of the instability and the Flame Response Rayleigh Index due to the secondary fuel. It is demonstrated that these results can be used to optimize the location and timing of the secondary fuel injection for maximum suppression of the instability.

Introduction

In order to meet increasingly stringent NOx emissions regulations, gas turbine manufacturers have been forced to abandon conventional diffusion flame based combustion strategies and replace them with lean premixed combustion strategies. The lower flame temperatures that are possible with lean premixed combustion have allowed for significant reductions in NOx emissions, however, this is at the expense of a substantially increased tendency for unstable combustion. To date there are no design methodologies that are capable of designing a lean premixed combustor which will be free of combustion dynamics over its entire operating range. It is not even possible to predict the operating conditions at which a given combustor will go unstable and the characteristics of the instability. As a result, instabilities are typically not encountered until the gas turbine is operating in the field. Once an instability has been demonstrated and characterized, then passive control strategies, such as the addition of acoustic damping, are implemented with varying degrees of success. This approach is time consuming, expensive and is usually not successful at eliminating all instabilities. An alternative to the use of passive techniques for suppressing unstable combustion is the use of active control techniques.

Suppression of combustion dynamics in gas turbine combustors using active combustion control has been successfully demonstrated in a number of laboratory-scale combustors[1-14] and in a few full-scale combustors[15-16]. The most successful applications have employed closed-loop control using main or secondary fuel modulation. The rationale behind this approach is that the modulated fuel is used to produce modulated heat release which is out of phase with the pressure oscillation, thereby increasing the system damping and suppressing the instability.

Two important practical considerations when using fuel modulation for active combustion control in a full-scale combustor are that the fuel flow rates are very large and the instability frequencies in gas turbine combustors are typically between 100 and 1000Hz. Although actuators that are capable of modulating large fuel flow rates at such frequencies are available, they are expensive and there are concerns regarding their durability. One approach for minimizing the actuator requirements is the use of subharmonic fuel modulation, which reduces the modulation frequency and in doing so also extends the lifetime of the actuator. A second approach is to use secondary fuel modulation instead of primary fuel modulation. This offers the potential to optimize the location of secondary fuel injection so as to achieve effective control with the minimum amount of fuel. Both of these approaches offer the potential for improving the viability of active combustion control for practical applications. In the first part of this paper, results are presented from a study of the use of secondary fuel with subharmonic modulation for the suppression of combustion dynamics. In the second part of this paper, results are presented from a study of the effect of secondary fuel injection location on the suppression of combustion dynamics.

Part 1 - Subharmonic Injection

Experiment (Part 1)

The apparatus used to study subharmonic injection is illustrated schematically in Fig. 1. The combustor was a laboratory-scale, coaxial dump combustor operating at a pressure of 100 kPa. It consists of an upstream stainless steel mixing section (12 mm i.d., 72 cm long) and a downstream quartz combustion section (42 mm i.d., 41 cm long). The mixing and combustion sections are joined by a brass junction piece, which also houses the secondary fuel injector. The quartz tube slides over the junction piece and ceramic insulation is used to fill the small gap between the two. A crosshair-type flame holder is fitted onto the brass junction piece and positioned about 5 mm downstream of the dump plane.

Methane was used as both the primary and the secondary fuel. The combustor was designed such that primary fuel can be delivered at two different locations. It can be introduced at the entrance to the mixing section (~60 mixing tube diameters upstream of the dump plane), or at a location six mixing tube diameters upstream of the dump plane through a 3.175 mm diameter tube located concentrically inside the mixing section. Fuel introduced at the entrance to the mixing section is assumed to be completely mixed by the time it reaches the combustion section, and fuel introduced through the concentric tube is considered to be incompletely or partially mixed. The primary fuel can be introduced at either of these locations or a combination of the two, which is denoted by the percent fuel split. For example, fuel entering entirely from 60 mixing tube diameters upstream of the dump plane would be referred to as a 100% fuel split, whereas the case when the fuel is divided equally between the two locations would be a 50% fuel split. Primary fuel flow rates ranged from 1 to 4 lpm. Using the higher heating value for methane, this corresponds to heat release rates from 0.7 to 2.8 kW.

The air was preheated by means of two 625 watt heating tapes. One heating tape was wrapped around a coiled 3.175 mm stainless steel tube prior to the mixing section. The second heating tape was wrapped around the mixing tube and then insulated with pipe insulation. The experiments were conducted over a temperature range of 400-500°C and over a bulk velocity of 6-10 m/s in the mixing section.

The control system is designed to observe the output of a microphone mounted next to the combustor exit, to determine when an instability occurs, and then to deliver short bursts of secondary fuel, which are phase-locked with the dominant frequency of the instability, until the pressure fluctuations are quelled. A schematic drawing of the control system is shown in Fig. 2. The primary components of the control system are 1) the sensor, which monitors the pressure fluctuations in the combustor; 2) the control circuit, which processes the signal from the sensor and sets the timing and the duration of the signal sent to the actuator; 3) the actuator, which receives the control signal from the control circuit, and then modulates the secondary fuel accordingly; and 4) the fuel injector, which delivers the fuel to the desired location in the combustor.

The sensor used in this experiment is a microphone-based sound level meter. This device provided a direct readout of the sound level in dB, as well as the output signal from the microphone that was used to monitor the pressure fluctuation. To ensure the consistency of the sound level measurement, the location and orientation of the sound level meter were held constant for all the experiments; i.e., normal to the exit of the quartz combustion tube, 15 cm from the centerline, and at the same height as the axis of the combustor.

The control circuit is comprised of three separate pieces of equipment: a signal amplifier, a signal processor, and a valve driver. The purpose of the signal processor is to determine the time of 0 degree phase in the pressure oscillation, and to provide that input to the valve driver. The valve driver (General Valve Iota One) is triggered by the rising edge of the valve driver trigger signal that is provided by the signal processor. The delay, relative to the time of 0 degree phase in the pressure oscillation, and the duration of the high voltage control signal, are set in the valve driver and sent to the actuator. The valve driver is capable of producing high voltage control signals as short as 250 μsec in duration at frequencies up to 250 Hz.

The actuator is a high frequency response solenoid valve (General Valve Series 9) which is capable of operating (using the Iota One Driver) at frequencies up to 250 Hz with open times as short as 250 μsec. From the valve, fuel travels through a 10 cm length of 1.59 mm i.d. tubing to the manifold in the secondary fuel injector. The total volume of the fuel tube and fuel manifold is ~ 4.4 cc, which is nominally 10 times the volume of injected fuel. From the fuel manifold, eight 0.8 mm diameter holes, angled toward the exit of the mixing section, direct secondary fuel towards the base of the flame (Fig. 2).

Using high speed shadowgraphy, the output of the secondary fuel injector was visualized at frequencies up to 200 Hz and control signal durations as short as 2 msec. Over this range of conditions, the valve output was found to accurately mimic the control signal, however, erratic behavior was observed when operated at frequencies near 200 Hz for prolonged periods of time, i.e., for more than one hour. Characterization of the valve's performance using control signal durations less than 2 msec was done by monitoring the time averaged flow rate through the valve as the frequency and duration of the control signal were varied. The results of these tests are shown in Fig. 3, where the flow rate versus the duration of the control signal is plotted for control signal frequencies of 25, 50 and 100 Hz. Figure 3 shows that the flow rate varied linearly with control signal durations as short as 300 μsec. This indicates that the fidelity between the control signal to the solenoid valve and the actual fuel pulse is maintained over this range of frequencies and durations.

Results and Discussion (Part 1)

The combustor was found to exhibit unstable combustion at a number of different operating conditions. For the purposes of this study, instabilities that occurred with a 50% fuel split, an

inlet temperature of 415°C, and a mixing section velocity of 9.0 m/s, at equivalence ratios from 0.5 to 1.0, were selected for use. The stability map for this operating range is shown in Fig. 4. The stability map is a plot of the dB reading of the sound level meter versus equivalence ratio for fixed fuel split, inlet temperature and mixing section velocity. As shown in Fig. 5, the combustor is unstable over the entire operating range, except at the leanest conditions. All of the instabilities that were observed exhibited a dominant frequency near 350 Hz as shown in the frequency spectrum presented in Fig. 5. This frequency agrees well with an estimate of the frequency of a quarter-wave standing wave in the combustor, indicating that the instability is a longitudinal mode instability.

Control experiments were conducted over the range of combustor operating conditions mentioned above. The experiments involved systematically varying a number of control parameters to determine the optimum level of control that could be achieved at each combustor operating condition. The control parameters that were varied included the secondary injection frequency; the phase angle between secondary fuel injection and the pressure oscillation in the combustor; the injection threshold, i.e., the minimum pressure level needed to trigger the control system; and the injection duration. The secondary fuel pressure was kept constant at 45 psia. The range of values over which the control parameters were varied is summarized in Table 1.

Table 1. Test range of control parameters.

Control Parameter	**Test Range**
Phase Angle	0-360 deg
Injection Threshold	0-100% of P_{p-p}*
Injection Frequency	1/2, 1/4, 1/8 and 1/16 instability frequency
Injection Duration	300-800 μsec
Injection Pressure	45 psia

* P_{p-p}, peak-to-peak pressure

Figure 6 depicts the typical initial control of an instability. The pressure wave and injector control signal are plotted versus time over a period of one second. From the time the controller is first turned on it takes approximately 600 msec for the instability to be suppressed with a secondary injection frequency of about 90 Hz, i.e., injecting every 4^{th} pressure cycle. After the instability is suppressed, the control only responds when the pressure wave begins to grow in intensity. In this case only seven secondary fuel injections over a period of 450 msec are necessary to keep the instability under control. This corresponds to an average injection frequency of only 15 Hz. The time it takes initially for the control to become effective varies with equivalence ratio. The instability is brought under control most rapidly at an equivalence ratio of 0.85. With increasing equivalence ratio, the time required to initially control the instability increases.

The frequency of fuel injection also plays a role in determining the length of the initial control time and the overall effectiveness of control. The control circuit is equipped with a frequency divider which divides the frequency of the instability by 2, 4, 8, or 16, i.e., the 1^{st}, 3^{rd}, 7^{th} and 15^{th} subharmonics, respectively. The resultant frequency is the control frequency. It was determined that 7^{th} and 15^{th} subharmonic injection were ineffective for all of the instabilities tested; while both 1^{st} and 3^{rd} subharmonic injection were effective, with the former being somewhat more effective.

As expected, the difference in phase between the start of secondary injection and the pressure oscillation in the combustor has a very significant effect on control effectiveness. The sound level versus phase angle plot for a typical operating condition is shown in Fig. 7. (Note that this is the phase angle between the pressure wave at the dump plane and the actual start of injection.) The phase angle has a positive effect over the range of 100 to 240 degrees. The mean sound level was reduced over this range, though the variance tended to be very large for some cases. Where the phase angle was not effective, the mean sound level increases because the secondary injection was actually feeding the instability. The optimum phase angle setting occurs at 205 degrees. This corresponds to fuel injection at a point slightly after the pressure peak. This optimum phase angle of 205 degrees was found to be the same over the range of operating conditions used in this study.

The effect of the threshold setting on control effectiveness is illustrated in Fig. 8, which is a plot of the combustor pressure and the actuator trigger signal over a one second interval for what are called a low, optimum and high threshold. In the low threshold case the greatest reduction on the pressure oscillation is observed, however, this requires the greatest number of secondary injections. In the high threshold case, the amplitude of the pressure fluctuations is noticeably greater than in the low threshold case and there are intermittent periods of large pressure fluctuations which require a significant number of injections to suppress. The optimum threshold setting can be defined as that corresponding to the greatest sound level reduction for the least amount of secondary fuel. For the optimum threshold setting case shown in Fig. 8, there is only a slight increase in the amplitude of the oscillations compared to the low threshold case, while there is a significant reduction in the number of injections. And compared to the high threshold case, the main difference is the absence of the intermittent periods of large pressure fluctuations that are observed with the high threshold.

Using 3rd subharmonic injection and the optimum threshold, duration and phase, the control effectiveness was determined at all of the unstable operating conditions shown in Fig. 4. These results are presented in the upper graph shown in Fig. 9, where the sound level meter reading as a function of equivalence ratio is plotted both with and without control. Over the range of equivalence ratios from 0.55 to 0.85, the most effective suppression of the instability was achieved with an almost 20 dB reduction in the sound level meter reading. At equivalence ratios above 0.85, control became less effective, and at stoichiometric conditions very little suppression (~2 dB) of the instability was observed.

Also shown in Fig. 9 (in the lower graph) is the amount of secondary fuel used to achieve control, expressed as a percentage of the primary fuel flow rate. The secondary fuel flow rate was calculated from the average number of secondary injections per second and the amount of fuel per injection, which was determined by the injection pressure and duration. A significant variation in the amount of secondary fuel that is required to suppress the instability is observed as the equivalence ratio is changed, even though the strength of the instability was relatively constant. At low and high equivalence ratios, the amount of secondary fuel required to suppress the instability approached an amount equal to 30% of the primary fuel; while at equivalence ratios near 0.8 only 2% secondary fuel was required to achieve a 22 dB reduction of the sound level meter reading. The fact that different amounts of secondary fuel were required to suppress the instability at different equivalence ratios can not be attributed to a change in the strength of the instability, which as noted above was relatively constant. This suggests that the characteristics of the instability changed with equivalence ratio such that the effectiveness of the secondary fuel also changed. This is addressed in more detail in the second part of this paper.

Conclusions (Part 1)

The use of closed loop active control based on secondary fuel injection at frequencies that are subharmonics of the frequency of the instability was studied. Experiments were conducted in a laboratory scale dump combustor that was designed with provision for secondary injection at the base of the dump plane. Tests were conducted at atmospheric pressure with an inlet temperature of 415°C, an inlet bulk velocity of 9.3 m/s, and over a range of overall equivalence ratios from lean blowout to stoichiometric. Unstable combustion occurred over an equivalence ratio range from 0.55 to 1.0, at frequencies around 350 Hz.

Control variables, such as phase angle, injection frequency, injection threshold, injection duration, and injection pressure were varied to evaluate their effect on the suppression of combustion generated oscillations and to determine optimum values for maximum sound level reduction with minimum secondary fuel. The most effective and efficient control was achieved at an equivalence ratio of 0.85, where a 22 dB sound level reduction was achieved using 2% secondary fuel. Of particular note is the fact that this was accomplished using an injection frequency that was one-fourth of the instability frequency, which has important practical implications in terms of reducing the need for high frequency actuation and for extending actuator lifetimes.

Part 2 - Effect of Injection Location on Control Effectiveness

Experiment (Part 2)

The laboratory-scale lean-premixed combustor used in this study consists of a mixing section and an optically-accessible combustion chamber as illustrated in Fig. 10. The flame is stabilized on a bluff centerbody (19mm dia.) which is flush-mounted with the combustor dump plane. The centerbody is supported in the mixing section (37mm i.d.) by a 30º axial swirler positioned 60mm upstream of the dump plane. The upstream end of the combustion chamber is made from a 110 mm i.d. fused-silica tube and the downstream end is fabricated from a 78 mm i.d. stainless steel pipe. The inlet to the mixing section is choked, while the combustor exit is partially restricted, thus providing well-defined inlet and outlet acoustic boundary conditions. The air flow is heated with an electric heater and its temperature is monitored by a thermocouple locatedin the mixing section. Natural gas (96 % methane) was used as the main and the secondary fuel. As illustrated in Fig. 11, the main fuel is introduced either directly into the annular mixing section (case I) or well upstream of the mixing section (case II). In case I, fuel is injected 25 mm upstream of the dump plane through sixteen 0.41 mm diameter holes equally-spaced around the centerbody, resulting in a non-uniform fuel distribution at the combustor inlet. In case II, fuel and air are mixed upstream of the choked inlet to the mixing section, giving a uniform fuel distribution at the combustor inlet.

Table 2. Operating conditions for the case I and case II instabilities

	Case I	Case II
Average velocity in combustor	5.25m/sec	
Average velocity in mixing section	70m/sec	
Overall equivalence ratio	0.575	
Inlet temperature	350°C	
Swirl number	0.46 (30° axial swirler)	
Mode of instability (frequency)	Longitudinal mode (360Hz)	
Amplitude of pressure fluctuation at peak frequency ($P_{peak\text{-}to\text{-}peak}/P_{mean}$ in %)	10.1 %	5.9 %

Two unstable operating conditions, described in Table 2, are chosen for this study. Both result in longitudinal mode instabilities at a frequency of ~360 Hz. The mixing section velocity, the combustor inlet temperature and the overall equivalence ratio are the same for the two instabilities. The only difference is the fuel injection location and the resulting fuel distribution at the combustor inlet, i.e., case I and case II described above.

The pressure fluctuation in the combustor is measured using a water-cooled piezoelectric pressure transducer mounted in the dump plane. The signal from the pressure transducer is used as a reference for the active control system.

In order to measure the temporal fluctuation of the overall heat release rate, CO_2* chemiluminescence emission[17] from the entire flame is detected using a photomultiplier tube (PMT) fitted with a broad band-pass filter (BG-40). In order to characterize the spatial and temporal evolution of the flame's heat release during unstable combustion, the chemiluminescence emission from the flame is imaged onto an intensified CCD (ICCD) camera fitted with a BG-40 filter. The chemiluminescence images are phase-synchronized with the pressure oscillation in the combustor. During one period of the instability fifteen phase-averaged images are acquired, each separated by 24 phase-angle degrees. Each phase-averaged image is an average of 30 instantaneous images recorded at the same phase-angle but in different cycles of the instability. The ICCD camera exposure time is 50μsec, which corresponds to less than 2% of the instability period. Because the chemiluminescence image is a line-of-sight measurement it does not reveal the interior structure of the flame[17]. By assuming that the flame is axisymmetric and applying a tomographic deconvolution procedure a two-dimensional image of the flame structure can be obtained.[17,18]

Laser induced acetone fluorescence is used to measure the main and secondary fuel distribution at the entrance to the combustor under non-combusting conditions.[17] For these measurements the fuel is replaced by nitrogen seeded with 0.5% by volume of acetone. The inlet air temperature for these measurements is set at 100°C to avoid condensation of acetone. The 266nm output of a frequency-quadrupled pulsed Nd:YAG laser is used as the excitation source and the resulting fluorescence is recorded using an ICCD camera, equipped with a band-pass filter (BG-12) and long-pass filter (WG305). In the case of modulated secondary fuel injection, the laser is phase-synchronized with the fuel injection cycle in order to obtain a sequence of images showing the spatial and temporal distribution of the injected fuel in the combustor during one injection cycle.

Active control is achieved using sub-harmonic injection of secondary fuel, where the frequency of injection is one-fourth the frequency of the instability, i.e., $f_{injection} = ¼\ f_{instability}$. The injection of secondary fuel is phase-synchronized with the pressure oscillation in the combustor and the phase-delay relative to the pressure oscillation is varied to achieve maximum suppression of the instability. The threshold is set so as to have injection on every 4^{th} cycle of the instability.

A pressure transducer mounted in the dump plane is used as the sensor for the control system. The amplified output of the pressure transducer is fed into a control circuit where a reference pulse is generated at the negative-to-positive zero-crossing of the pressure signal. The reference pulse is input to an actuator driver (General Valve Co., Iota One) where the injection duration of the actuator and the phase-delay between the pressure signal and the trigger input to the actuator are set. The actuator is a high-frequency response solenoid valve (General Valve Co., Series 9). The injection pressure for the secondary fuel, measured upstream of the actuator, is fixed at 150 psig and the amount of secondary fuel per injection is

varied by changing the injection duration.

As shown in Fig. 11, secondary fuel can be injected at one of two locations. The first is through twelve 0.34 mm diameter holes located around the inner circumference of the dump plane and is referred to as dump plane injection. The second is through four 1.40 mm diameter holes located in the outer wall of the mixing section and referred to as upstream injection. In the case of dump plane injection, secondary fuel is injected directly into the combustor. In the case of upstream injection, the secondary fuel is injected into the mixing section, approximately 110 mm upstream of the dump plane.

Results and Discussion (Part 2)

Figure 12 shows the effectiveness of control versus secondary injection phase-delay for the case I and case II instabilities for both secondary fuel injection locations, i.e., dump plane and upstream. Control effectiveness is defined as the reduction of the rms pressure fluctuation with respect to that of the unstable flame and the phase-delay represents the time delay between the zero-crossing of the combustor pressure signal and the trigger input to the actuator. Results are presented for injection-durations of 600, 1000 and 1200 microseconds, which correspond to secondary fuel flow rates that are 4.2%, 5.2% and 6.6% of the main fuel flow rate, respectively. These results show that control effectiveness depends not only on the phase delay and amount of injected fuel, but also on the location of secondary fuel injection. For the case I instability, dump plane injection results in the most effective control with a 21 dB reduction for a phase delay of 1.0 msec, while upstream injection has virtually no effect on the case I instability. For the case II instability the results are reversed and upstream injection is more effective than dump plane injection, i.e., upstream injection results in a 13 dB reduction for a phase delay of 2.5msec compared to a best case reduction of 1.6 dB with dump plane injection. In order to explain this behavior, the detailed characteristics of the unstable flames and of the injected secondary fuel are presented in the following sections.

For the case I instability, main fuel is injected directly into the mixing section through holes in the centerbody, as illustrated in Fig. 11. For the case II instability, main fuel is mixed with the air upstream of the choked inlet to the mixing section. The fuel distribution at the inlet to the combustor is measured using laser induced acetone fluorescence, as discussed previously, and the results for case I and case II are shown in Fig. 13. These results are averages of 40 instantaneous measurements. As expected, the fuel distribution in case II is uniform. In case I, however, the equivalence ratio varies almost linearly from 0.25 to 0.95 across the annular mixing section. The case I fuel distribution is also measured at different azimuthal angles by rotating the centerbody and the results show that the fuel distribution is axisymmetric to within ±15%.

Figures 14(a) and 14(b) show the sequence of phase-averaged, two-dimensional chemiluminescence images during one period of unstable combustion for the case I and II instabilities, respectively. Each image is displayed in gray-scale where the chemiluminescence intensity increases from black to white. Only the upper half of each image is shown (since the deconvoluted images are axisymmetric) and to the left of each image is a schematic representation of the dump plane, the centerbody and the annular mixing section. The pressure oscillation measured at the dump plane is plotted for each set of images with frame number referring to the moment when the image is taken. For both cases, the maximum and minimum chemiluminescence intensity occur approximately at the same time as the maximum and minimum pressure, respectively, indicating that the pressure and heat release fluctuations are very nearly in phase. Each set of chemiluminescence images

show clear evidence of periodic vortex shedding and the subsequent interaction with the flame. However, the details of the interaction are noticeably different in the two cases, i.e., in case I the reaction appears to be contained within the vortex, whereas the flame appears to be wrapped around the vortex in case II.

The differences between the instabilities are more apparent when the local Rayleigh Index distributions are compared. The local Rayleigh Index quantifies the strength of the coupling between the local unsteady heat release and the local acoustic pressure fluctuations, and for the axisymmetric flame is given by

$$R(r, z) = \frac{1}{T}\int^{T} p'(r,z,t)q'(r,z,t)dt$$

where t is time, r and z define the radial and axial location in the combustor, respectively, T is the instability period, p' is the local pressure fluctuation and q' is the local heat release fluctuation. The local Rayleigh Index distribution identifies regions in the combustor where either driving or damping of the instability occurs, as indicated by positive or negative values of the local Rayleigh Index, respectively. Using the local chemiluminescence intensity as an indicator of the local heat release and noting that the length of the flame zone (<10 cm) is much smaller than the acoustic wavelength (~200 cm for both cases), the local Rayleigh Index distribution can be calculated from the phase-averaged chemiluminescence images and the pressure oscillation measured at the dump plane.

The local Rayleigh Index distributions for the case I and case II instabilities are shown in Fig. 15(a) and 15(b), respectively. As shown in Fig. 15(a), the case I instability has two damping regions, one close to the “shoulder” of the dump plane and another along the centerline of the combustor immediately downstream of the centerbody. A negative Rayleigh index is the result of heat release occurring when the pressure is at or near its minimum, as is shown in images (5) through (7) of Fig 14(a). Inspection of these images shows that the maximum heat release at the time of minimum pressure occurs near the shoulder of the dump plane, which is consistent with the fact that this is a region of significant damping. There is also evidence of heat release along the centerline of the combustor immediately downstream of the centerbody, which coincides with the smaller and weaker damping region at this location. Figure 15(a) also shows that the region where driving is strongest is located further downstream and close to the wall of the combustor.

For the case II instability, there are again two damping regions as shown in Fig. 15(b). One is located at the same radial position as the case I instability but about twice as far downstream of the dump plane. The other damping region is located immediately downstream of the centerbody. Inspection of images (4), (5) and (6) in Fig. 14(b) shows that at the time of minimum pressure the maximum heat release occurs at these locations. Similarly a positive local Rayleigh Index is due to local heat release occurring when the pressure is at or near its maximum as shown in images (11) through (13) of Figures 14(a) and 14(b). Inspection of these images shows that the location of maximum heat release at the time of maximum pressure coincides with the location of the maximum local Rayleigh Index shown in Figures 15(a) and 15(b).

Secondary fuel injection is characterized in terms of the spatial and temporal distribution of the fuel as it enters the combustor and in terms of the so-called flame response function.

The secondary fuel distribution is measured using laser induced acetone fluorescence, as described previously. In this case the laser beam is aligned so as to pass across the center of one of the dump plane injection holes at a distance 2 mm downstream of the dump plane and

the fluorescence image is acquired by an ICCD camera. Fuel distribution results for dump plane and upstream secondary injection are shown in Figures 16(a) and 16(b), respectively, for an injection duration of 1000 μsec. Figure 16 shows the fluorescence intensity, which is proportional to the fuel concentration, versus radial position at five different times after the trigger signal to the actuator. The space between two rectangles to the left of each graph indicates the location of the annular mixing section. In the case of dump plane injection, i.e., Fig. 16(a), the secondary fuel is concentrated at the injection site which is indicated by the arrow; whereas in the case of upstream injection, i.e., Fig. 16(b), the secondary fuel is distributed across the annular mixing section with a maximum concentration near the outer wall of the mixing section. These results also show that the duration of the secondary fuel pulse entering the combustor is approximately 3 msec and 2 msec for the dump plane and upstream injection case, respectively, whereas the pulse duration of the trigger signal to the solenoid valve is 1 msec, indicating that there is a significant spreading of the fuel pulse from the solenoid valve to where it enters the combustor.

The flame response function refers to the change in the flame's heat release due to secondary fuel injection. The flame's heat release is measured by detecting the intensity of the CO_2* chemiluminescence emission, as discussed previously, and the flame response function is the difference between the chemiluminescence intensity with and without secondary fuel injection. The flame response function is measured in a stable flame at the same inlet flow conditions as listed in Table 1, which is achieved by operating the combustor with one half of the main fuel flow injected through the centerbody and the other half upstream of the choked mixing section inlet.

The flame response function measurements for the two injection locations are shown in Figures 17(a) and 17(b). Each figure shows the temporal variation of modulated chemiluminescence intensity due to secondary fuel injection for three different injection durations, i.e., 600, 1000 and 1200 μsec. The time is referenced to the actuator input signal. In all cases the flame response function shows a sharp initial increase of chemiluminescence intensity followed by a gradual decrease. In the case of dump plane injection the sharp increase begins approximately 3 msec after the actuator signal and in the upstream injection case about 5 msec.

Assuming that the instability can be suppressed by out-of-phase heat addition, the relative effectiveness of secondary fuel injection can be estimated by comparing the Flame Response Rayleigh Index, which is defined as follows:

$$\text{Flame Response Rayleigh Index} = \frac{1}{\tau}\int_{t_o}^{t_o+\tau} p' q'_{\text{sec}ondary}\, dt$$

where τ is the secondary fuel injection period, t_o is the time delay between the rising edge of actuator trigger signal and the positive-to-negative zero-crossing of the pressure oscillation, p' is the measured pressure signal and $q'_{\text{secondary}}$ is the modulated heat release due to secondary fuel injection, i.e. the flame response function. The Flame Response Rayleigh Index is a measure of the effect of heat release due to secondary fuel on the instability. In order to illustrate how the Flame Response Rayleigh Index is calculated, the flame response function superimposed on the pressure oscillation is shown in Fig. 18. As t_o is varied, the value of the Flame Response Rayleigh Index varies, reflecting a change in control effectiveness. If the Flame Response Rayleigh Index is positive, secondary fuel injection should amplify the instability whereas the instability should be damped if the Flame Response Rayleigh Index is negative.

Figure 19 shows the Flame Response Rayleigh Index versus time delay for four cases, i.e.,

case I and II instabilities, each with dump plane and upstream secondary injection. In all four cases results for injection durations of 600, 1000 and 1200 μsec are shown. The time delay is varied over one period of the instability, i.e., approximately 2.7 msec. For a given injection location, maximum damping occurs at very nearly the same time delay for the two instabilities. This is because the instability frequency is nearly the same for both instabilities. With dump plane injection, for both instabilities, maximum damping is predicted to occur when the time delay is approximately 1.2 -1.5 msec, depending on the injection duration, i.e., the amount of secondary fuel. While with upstream injection, the time delay for maximum damping is predicted to occur with time delays of approximately 2.6-3.0 msec, again depending on the injection duration. The amount of damping is shown to increase with increasing injection duration, i.e., with increasing amount of fuel injected, in all cases.

Comparing the predicted optimum time delays indicated in Fig.19 with the actual control effectiveness results shown in Fig. 12 reveals a number of similarities and differences. The main similarity is that for the case I instability with dump plane injection and the case II instability with upstream injection, there is good agreement between the measured and predicted time delay for maximum damping and control. For the case I instability with dump plane injection, maximum damping is predicted for a time delay of between 1.2 and 1.5 msec, whereas the most effective control is observed experimentally with a time delay of 1.0 msec. For the case II instability with upstream injection, maximum damping is predicted for a time delay of between 2.6 and 3.0 msec, while the most effective control is observed experimentally with a the time delay of 2.5 msec. This suggests that the Flame Response Rayleigh Index provides a reasonably good estimation of the time delay required for optimum control.

The main difference between the Flame Response Rayleigh Index predictions and the experimentally observed control effectiveness is that the instability is not suppressed for the case I instability with upstream injection nor for the case II instability with dump plane injection, even at the time delays predicted to produce the greatest damping. This is not surprising, however, since the Flame Response Rayleigh Index only predicts the time delay for maximum damping, and does not predict whether that amount of damping is sufficient to suppress the instability. On the other hand, it is interesting to note that the time delay (i.e., approximately 2.8 msec) at which modulated secondary fuel injection is predicted to drive the instability for the case II instability with dump plane injection that in fact an increase in the pressure fluctuations is observed.

The spatial and temporal evolution of the unstable flame shown in Fig. 14, the Rayleigh Index distribution shown in Fig. 15 and the secondary fuel distribution shown in Fig. 16 suggest another explanation as to why secondary fuel injection from the dump plane is effective at controlling the case I instability while upstream injection is not. As discussed previously, in order for the secondary fuel to produce damping, the heat release due to the secondary fuel should occur when the pressure oscillation is near its minimum, which corresponds to images (5), (6) and (7) in Fig. 14(a). These images show that at the time of minimum pressure the reaction is occurring in a small region almost directly in front of the dump plane injection holes. Therefore, secondary fuel injected from the dump plane is injected directly into this region where it is quickly burned, resulting in maximum damping. On the other hand, secondary fuel injected at the upstream injection location enters the combustion chamber through the annular mixing section and must travel around the periphery of the vortex before reaching the region where combustion is occurring at the time of minimum pressure. As a result the secondary fuel burns more slowly, resulting in less damping. Another way of saying this is that the optimum injection location is one which most effectively introduces the secondary fuel into the region of maximum damping (as identified

by the Rayleigh Index distribution) since this is the location where combustion is occurring (hence an ignition source exists) at the time of minimum pressure.

This same reasoning can be applied to explain the control effectiveness results for the case II instability where, contrary to the case I instability, dump plane injection is not effective while upstream injection is. Images (4), (5) and (6) in Fig. 14(b) show that when the pressure oscillation is near its minimum there are two regions of intense combustion. One is located almost directly downstream of the annular exit of the mixing section and the other is located further downstream and closer to the outer wall of the combustor. The former region is located at the exit of the annular mixing section where secondary fuel is concentrated when injected from the upstream location. This ensures rapid heat release while the pressure is near its minimum, producing maximum damping. On the other hand, secondary fuel injected from the dump plane location can not readily access either of the regions of intense combustion at the time of minimum pressure and therefore will burn more slowly, resulting in less damping. Again the most effective control is achieved when the secondary fuel is introduced directly into the instability damping region as indicated by the Rayleigh Index distribution of the unstable flame in question.

Conclusions (Part 2)

The effective suppression of unstable combustion using modulated secondary fuel injection depends on the location as well as the timing of the secondary fuel injection. The flame response function for a particular secondary injection location can be used to calculate the Flame Response Rayleigh Index from which the optimum injection timing required for the maximum damping can be determined. Although the optimum timing of secondary fuel injection is critical, it is not sufficient to ensure the suppression of a given instability. One must also consider the spatial and temporal distribution of the injected secondary fuel relative to the spatial and temporal evolution of the unstable flame, since the interaction between the two can have a significant effect on the effectiveness of control. The results of this study indicate that the most effective control for a given instability is achieved by injecting the secondary fuel into a damping region identified in the Rayleigh Index distribution for the instability of interest so that rapid combustion of the secondary fuel is ensured while the pressure is near its minimum.

Acknowledgements

This research was conducted with support from the Office of Naval Research under Contract #N00014096-1-0405.

References

[1] Langhorne, P.J., Dowling, A.P. and Hooper, N., "Practical Active Control System for Combustion Oscillations," *Journal of Propulsion*, Vol. 6, pp. 324-333, 1990.

[2] Schadow, K.C., Gutmark, E. and Wilson, K.J., "Active Combustion Control in a Coaxial Dump Combustor," *Combustion Science and Technology*, Vol. 81, pp. 285-300, 1992.

[3] Poinsot, T.J., Bourienne, F., Candel, S., Esposito, E., Lang, W., "Suppression of Combustion Instabilities by Active Control," *Journal of Propulsion and Power*, Vol. 5, No. 1, pp. 14-20, 1989.

[4] Billoud, G., Galland, M.A., Huu, C.H. and Candel, S., "Adaptive Active Control of Combustion Instabilities," *Combustion Science and Technology*, Vol. 81, pp. 257-283, 1992.
[5] McManus, K.R., Poinsot, T., and Candel, S., "A Review of Active Control of Combustion Instabilities," *Combustion Science and Technology*, Vol. 105, pp. 1-29, 1993.
[6] Sivasegaram., S., Tsai, R.F. and Whitelaw, J.H., "Control of Combustion Oscillations by Forced Oscillation of Part of the Fuel Supply," *Combustion Science and Technology*, Vol. 105, pp. 67-83, 1995.
[7] Neumeier, Y. and Zinn, B.T., "Experimental Demonstration of Active Control of Combustion Instabilities Using Real-Time Modes Observation and Secondary Fuel Injection," *Proceedings of the Twenty-Sixth Symposium (International) on Combustion*, The Combustion Institute, pp. 2811-2818, 1996.
[8] Richards, G.A., Yip, M.J., Robey, E., Cowell, L. and Rawlins, D., "Combustion Oscillation Control by Cyclic Fuel Injection," ASME *Journal of Engineering for Gas Turbines and Power*, Vol. 119, pp.340-343, 1997
[9] Yu, K. H., Wilson, K. J. and Schadow, K. C., "Liquid-Fueled Active Instability Suppression," *Proceedings of the Twenty-seventh Symposium (International) on Combustion*, The Combustion Institute, pp. 2039-2046, 1998.
[10] Hathout, J.P., Fleifil, M., Annaswamy, A.M, and Ghoniem, A.F., "Combustion Instability Active Control Using Periodic Fuel Injection," *Journal of Propulsion and Power, Vol. 18, No. 2, pp. 390-399, 2002.*
[11] H. Sato, Y. Yasunami, S. Ogawa, and A.K. Hayashi, "Optimization of Oscillatory Flame in a Swirler Combustor Using an Active Control Method," 42nd AIAA Aerospace Sciences Meeting and Exhibit, Paper No. AIAA-2004-0640, 2004.
[12] Jones, C. M., Lee, J. G. and Santavicca, D. A., "Closed-loop Active Control of Combustion Instabilities Using Subharmonic Secondary Fuel Injection," *Journal of Propulsion and Power*, Vol. 15, pp. 584-590, 1999.
[13] Cohen, J.M., Stufflebeam, J.H. and Proscia, W., "The Effect of Fuel/Air Mixing on Actuation Authority in an Active Combustion Instability Control System," *Journal of Engineering for Gas Turbines and Power*, Vol. 123, pp. 537-542, 2001.
[14] Lee, J. G., Kim, K. and Santavicca, D. A., "Effect of Injection Location on the Effectiveness of an Active Control System Using Secondary Fuel Injection," *Proceedings of the Twenty-Eighth Symposium (International) on Combustion*, The Combustion Institute, pp. 739-746, 2000.
[15] Seume, J. R., Vortmeyer, N., Krause, W., Hermann, J., Hantschk, C. -C., Zangl, P., Gleis, S., Vortmeyer, D. and Orthmann, A., "Application of Active Combustion Control to a Heavy Duty Gas Turbine," ASME *Journal of Engineering for Gas Turbines and Power*, Vol. 120, N. 4, pp. 721-726, 1998.
[16] Hibshman, J. R., Cohen, J. M., Banaszuk, A., Anderson, T. A. and Alholm, "Active Control of Combustion Instability in a Liquid-Fueled Sector Combustor," ASME Paper 99-GT-215, 1999.
[17] Lee, J.G. and D.A. Santavicca, "Experimental Diagnostics for the Study of Combustion Instabilities in Lean Premixed Combustors," *Journal of Propulsion and Power*, Vol. 19, No. 5, pp. 735-749, 2003.
[18] Dasch, C.J., "One-Dimensional Tomography: A Comparison of Abel, Onion-Peeling, and Filtered Backprojection Methods," Applied Optics, Vol. 31, No. 8, pp. 1146-1152, 1992.

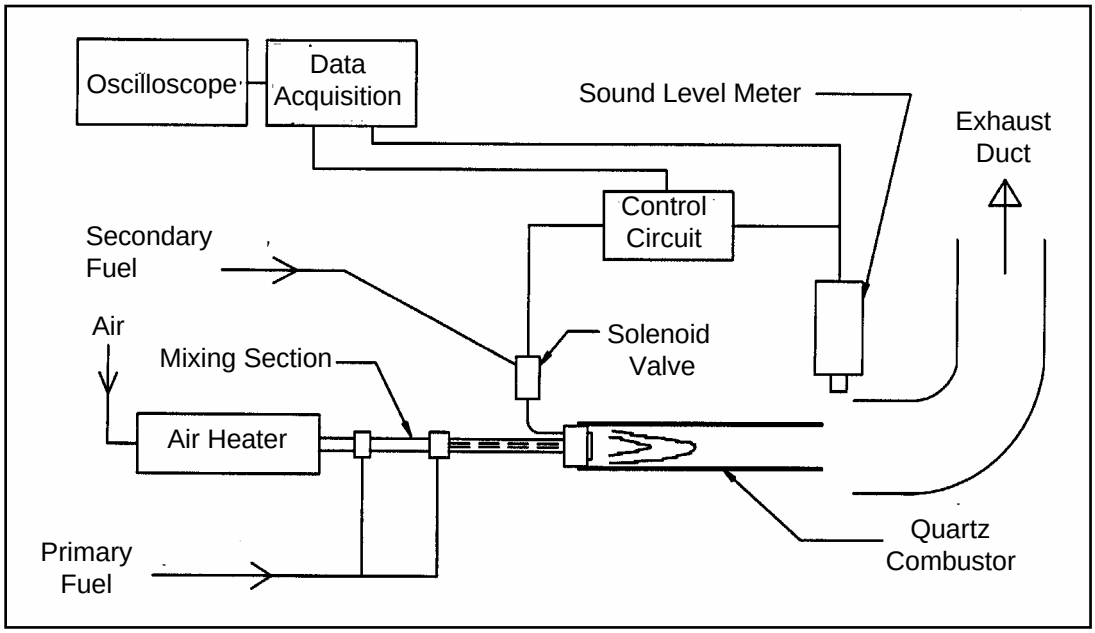

Figure 1. Schematic of test apparatus.

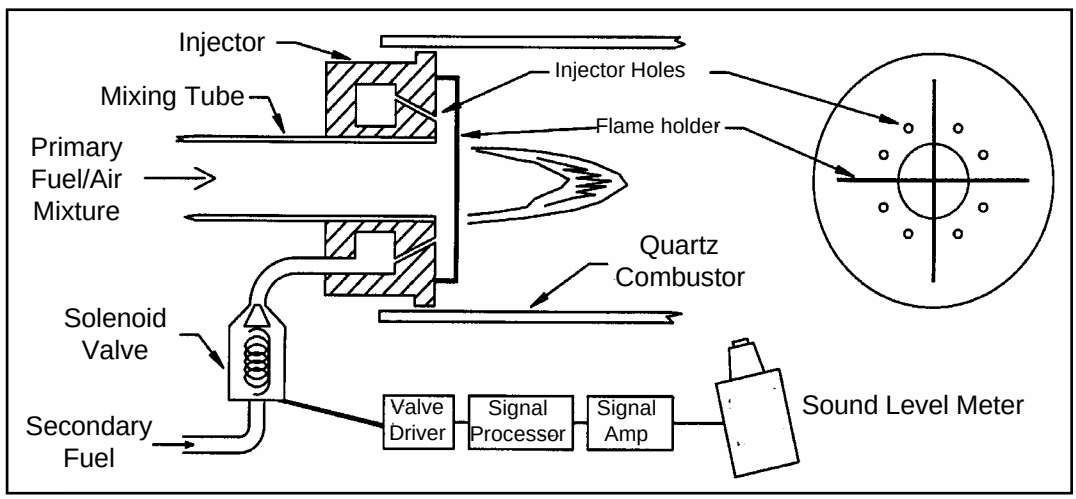

Figure 2. Control system configuration.

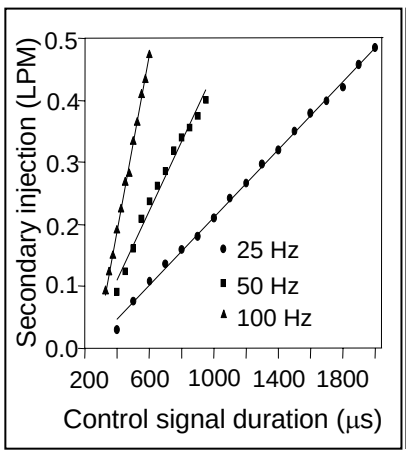

Figure 3 . Secondary injection flow rate versus control signal duration.

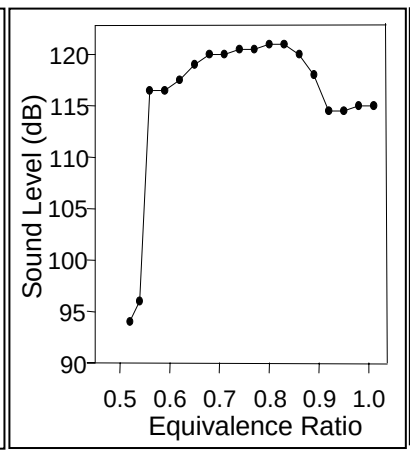

Figure 4. Instability map at T_{in}= 415°C and V_{in}= 9.5 m/s.

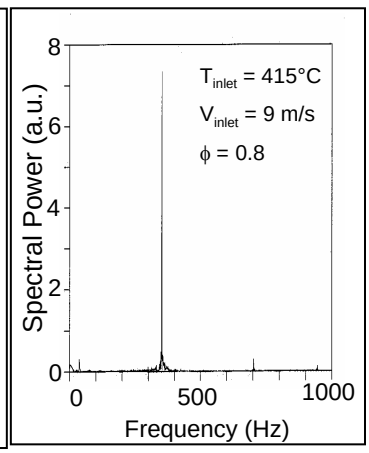

Figure 5. Frequency spectrum of unstable flame.

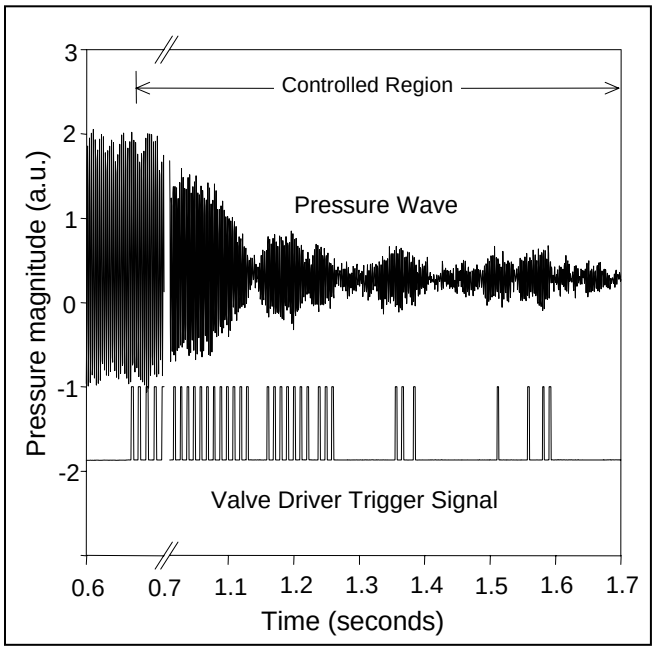

Figure 6. Pressure signal and valve driver signal vs. time during initial control of an instability.

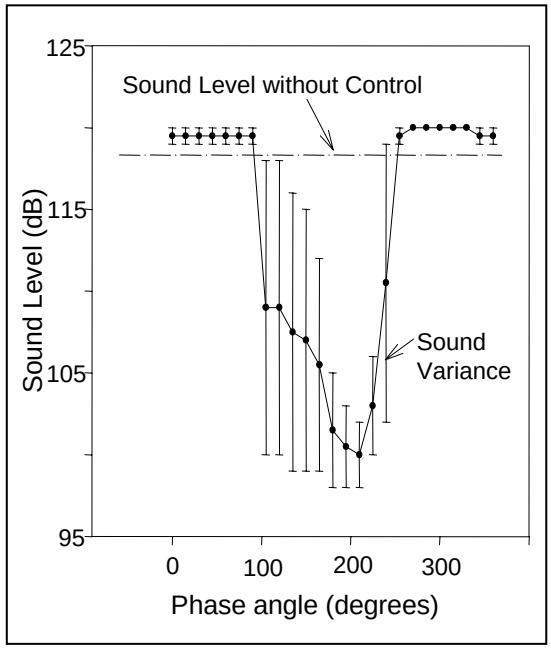

Figure 7. Sound level meter reading vs. phase delay.

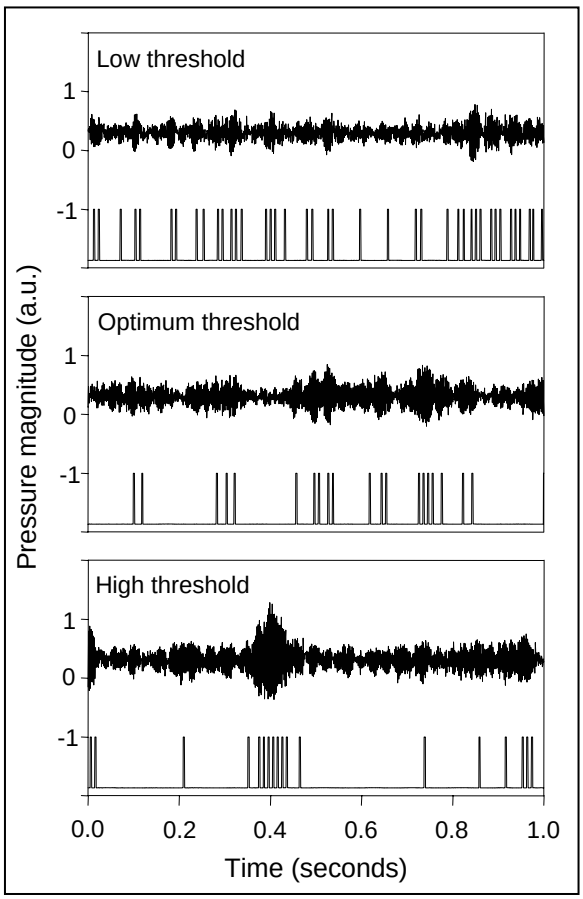

Figure 8. Pressure signal and valve driver signal vs. time for three threshold settings.

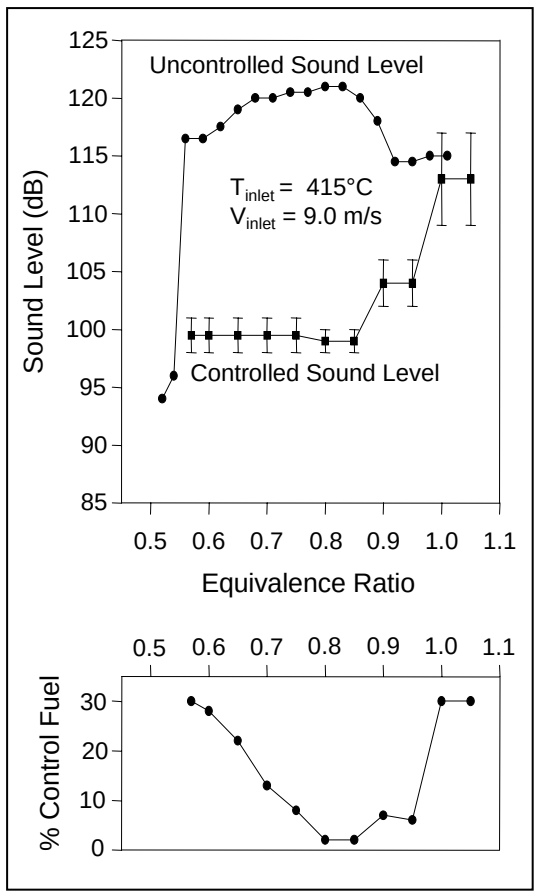

Figure 9. Maximum sound level reduction and percent secondary fuel vs. equivalence ratio.

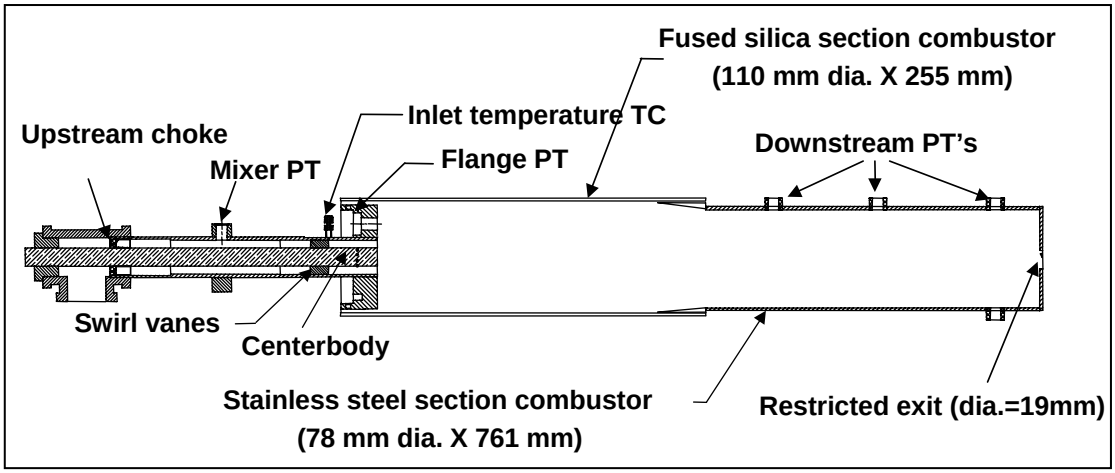

Figure 10. Schematic drawing of optically accessible dump combustor (not to scale).

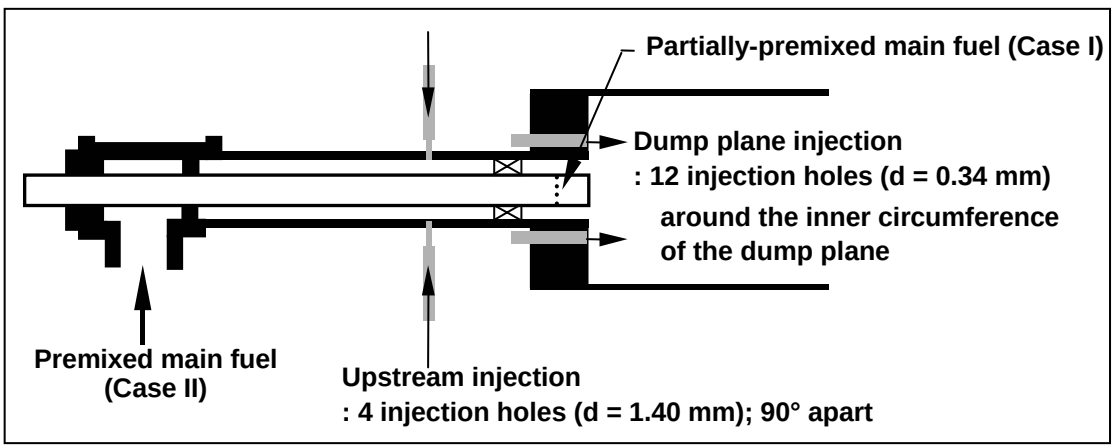

Figure 11. Schematic drawing showing both main and secondary fuel injection locations (not to scale).

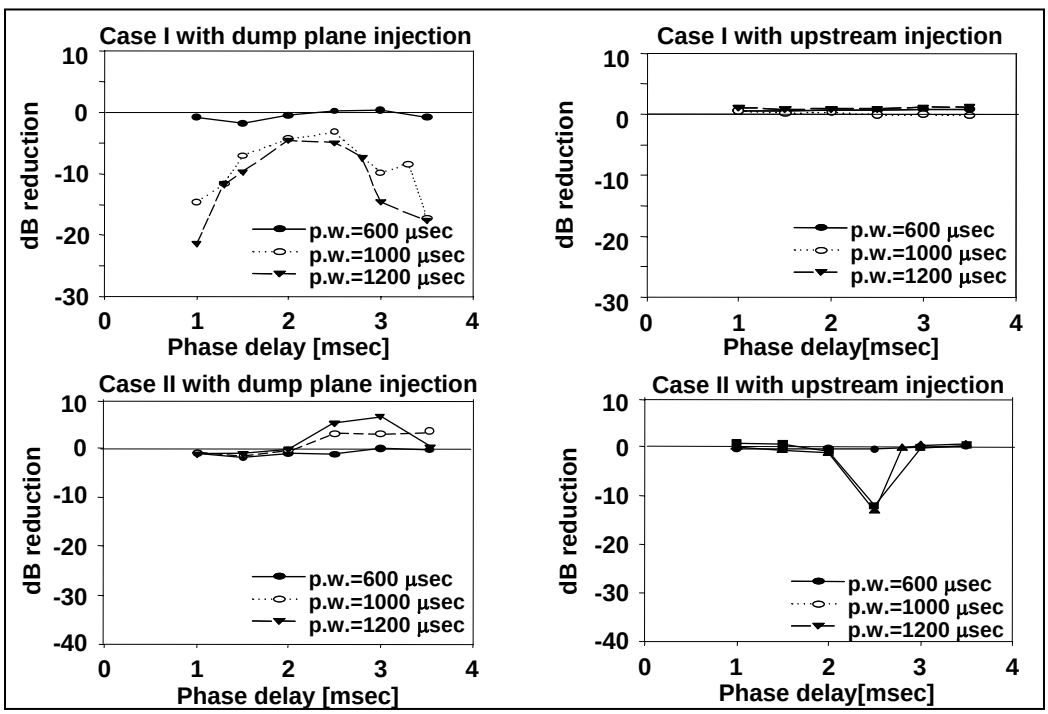

Figure 12. Control effectiveness vs. phase-delay for the case I and case II instabilities with dump plane and upstream injection.

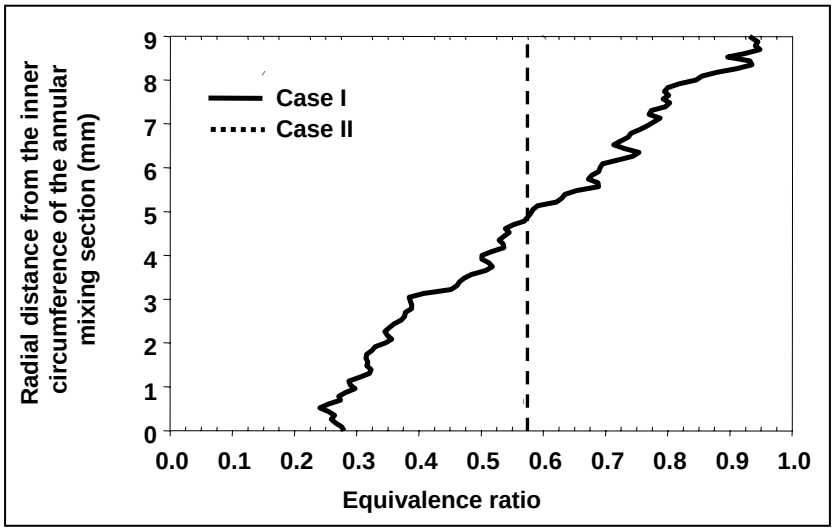

Figure 13. Combustor inlet main fuel distributions across the annular mixing section for case I and case II.

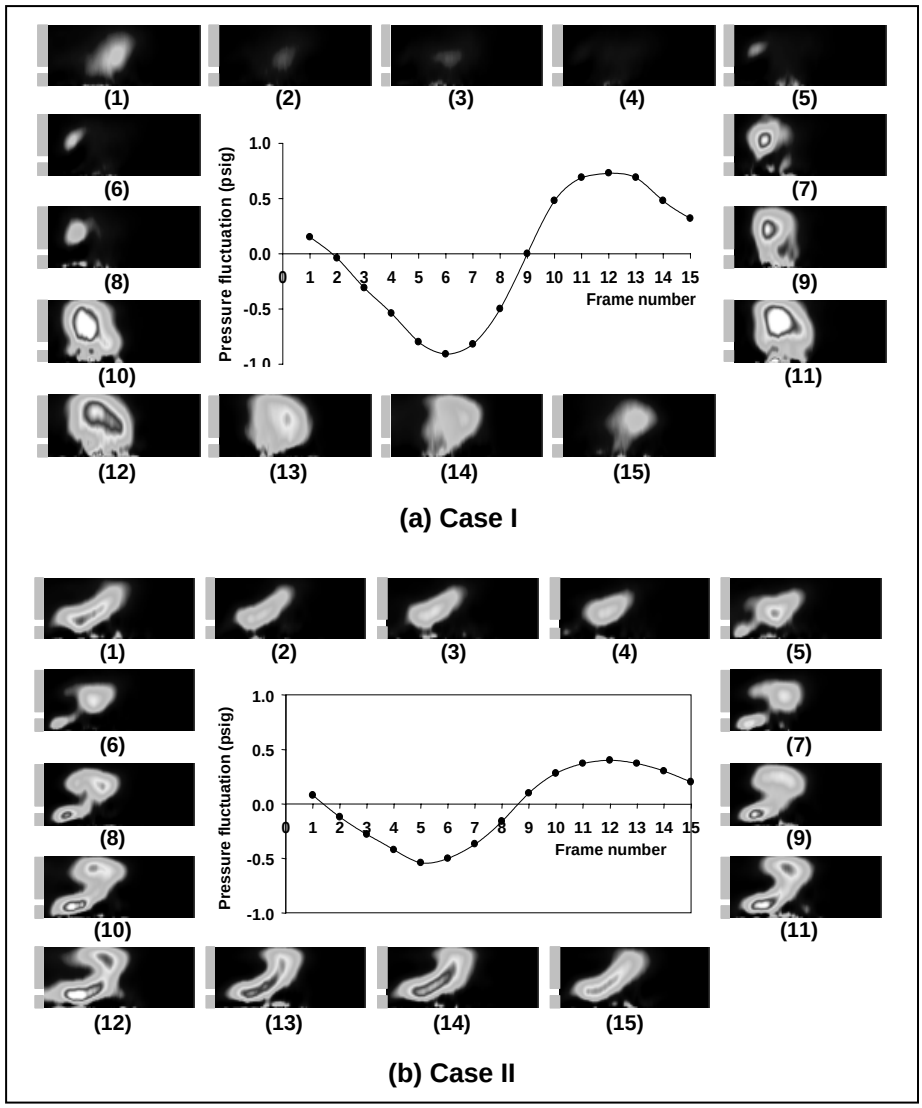

Figure 14. Two-dimensional chemiluminescence image sequences for (a) case I and (b) case II instabilities (The two lines to the left of each figure indicate the location of the annular entrance from the mixing section into the combustor.)

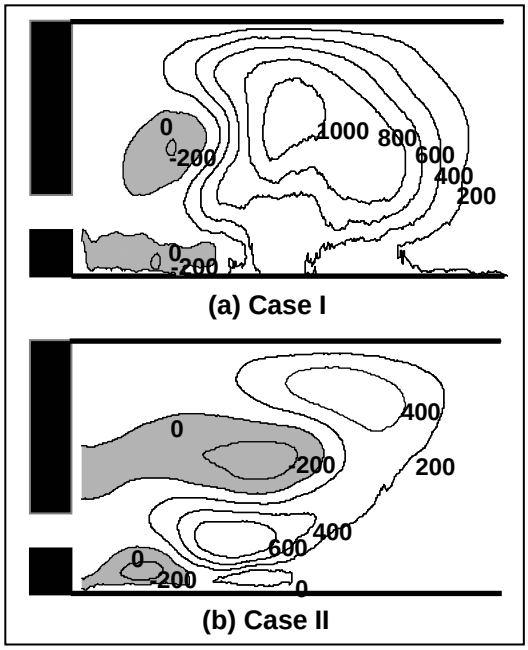

Figure 15. Rayleigh index distributions for (a) case I and (b) case II instabilities.

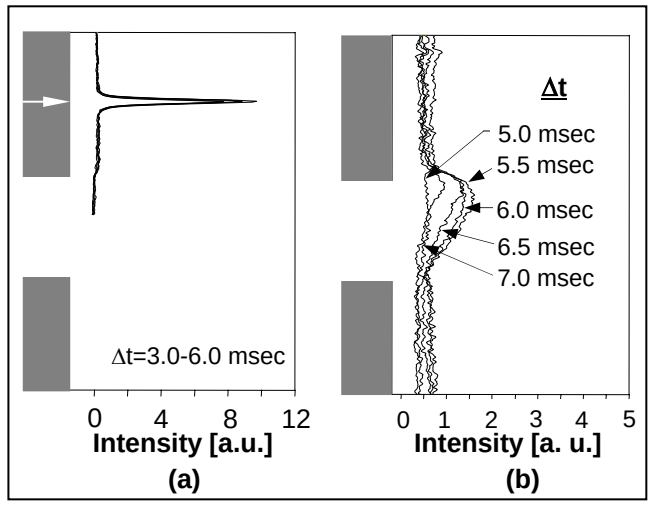

Figure 16. Spatial and temporal distribution of secondary fuel with (a) dump plane injection and (b) upstream injection (Dt represents the time delay between the time when the measurement is made and the rising edge of the trigger signal to the actuator)

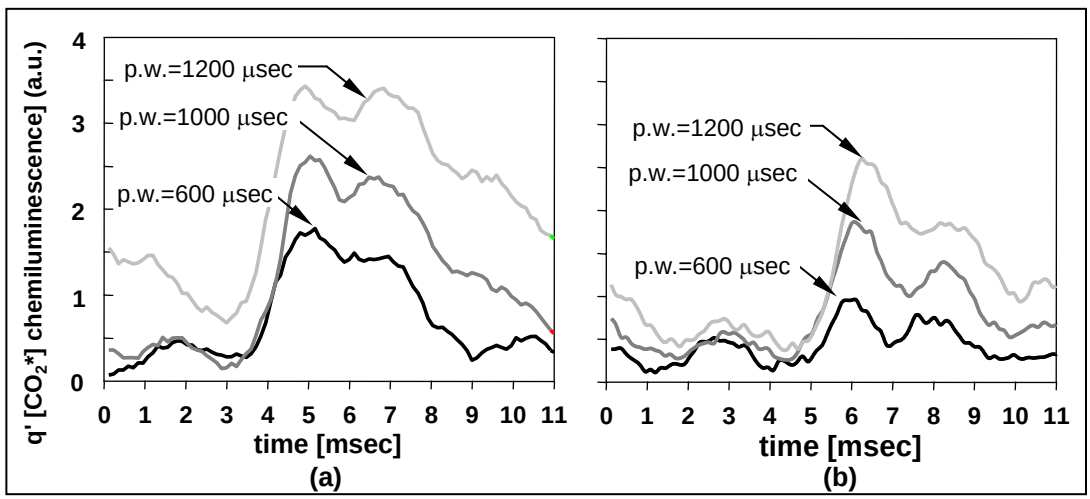

Figure 17. Flame response function measurements for (a) dump plane and (b) upstream injection.

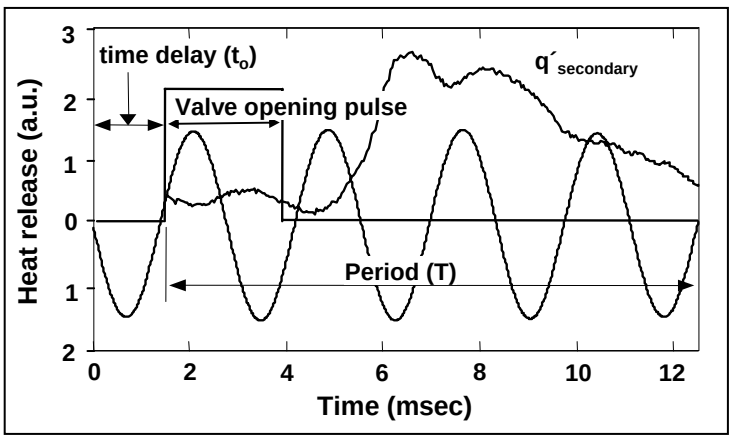

Figure 18. Flame response measurement for dump plane injection superimposed on the pressure trace.

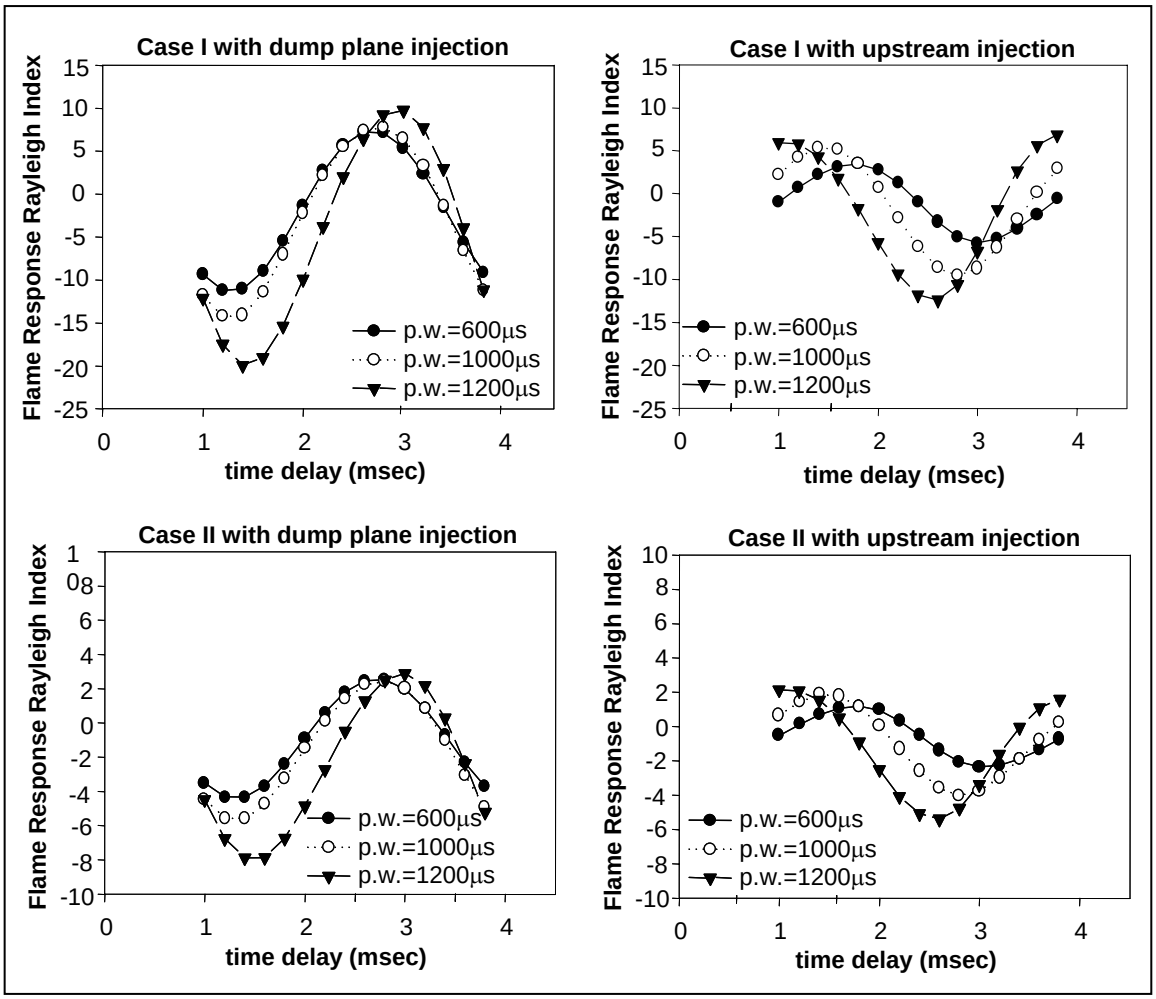

Figure 19. Flame Response Rayleigh Index versus time delay prediction for case I and case II instabilities with dump plane and upstream injection.